Dynamic Mode Decomposition of Unsteady Pressure-Sensitive Paint Measurements for the NASA Unitary Plan Wind Tunnel Tests

Jie Li[1], E. Lara Lash[2], Nettie H. Roozeboom[2], Theodore J. Garbeff[2], Christopher E. Henze[2], David D. Murakami[2], Nathanial T. Smith[1], Jennifer K. Baerny[2], Lawrence A. Hand[2], Marc A. Shaw-Lecerf[2], Paul M. Stremel[3], Lucy Z. Tang[1]

[1]Metis Technology Solutions, Inc.
Moffett Field, CA 94035

[2] NASA Ames Research Center
Moffett Field, CA 94035

[3]Science and Technology Corporation
Moffett Field, CA 94035

This paper discusses the Dynamic Mode Decomposition (DMD) of the Unsteady Pressure-Sensitive Paint (uPSP) measurements, which were collected with four Phantom high-speed cameras at a constant sample frequency in the Ascent Transient Aerodynamics Test (ATAT) of the Space Launch System (SLS) Block 1 cargo vehicle with the Unitary Plan Wind Tunnel (UPWT) 11-by-11-foot Transonic Wind Tunnel in September 2019 at NASA Ames Research Center. The conventional DMD algorithm is based on the Singular Value Decomposition (SVD). For the data with zero mean, the DMD is equivalent to the Discrete Fourier Transform (DFT). Since the uPSP is mainly used to determine the unsteady property of the aerodynamic flow, the DMD of the uPSP measurements is implemented in two steps: (1) subtract the mean value from the uPSP measurement; (2) apply the Fast Fourier Transform (FFT) on the resulting data with zero mean. The DMD of the uPSP measurements with FFT has two advantages: (1) the FFT algorithm is well known for its computational efficiency, therefore, compared to the SVD-based DMD algorithm, the DMD with FFT reduces the computation time; (2) the DMD with FFT can be easily implemented in parallel processing. The DMD outputs were generated with the execution in parallel of a code in C, with libraries of FFTW for FFT and MPI/OpenMP for parallel processing, on the NASA Pleiades supercomputer. In this paper, the results of DMD of the uPSP measurements in the tests of Mach sweep runs of the SLS ATAT are presented, and the effectiveness of the DMD of the uPSP measurements in the diagnosis of the unsteady, aerodynamic phenomena is demonstrated. The work described in this paper is a part of NASA's development of a new state-of-the-art uPSP capability in production wind tunnels. Funding for this research was provided by the NASA Aeroscience Evaluation and Test Capabilities Project.

Nomenclature

A	= DMD dynamics matrix
$\tilde{A}$	= proxy matrix
ATAT	= Ascent Transient Aerodynamics Test
D	= data matrix

DFT = Discrete Fourier Transform
DMD = Dynamic Mode Decomposition
FFT = Fast Fourier Transform
$f_{Nyquist}$ = Nyquist frequency
f_s = sample frequency
M = dimension of data vectors
N = number of data vectors
PSP = Pressure-Sensitive Paint
SLS = Space Launch System
SRB = Solid Rocket Booster
SVD = Singular Value Decomposition
UPWT = NASA Unitary Plan Wind Tunnel
U_r, Σ_r, V_r^T = output matrices of the reduced SVD of X
uPSP = Unsteady Pressure-Sensitive Paint
v = eigenvector of the DMD dynamics matrix
$\tilde{v}$ = eigenvector of the proxy matrix
W = vector of the DFT coefficients of the data matrix
$X, X^{\#}$ = matrices of data vectors defining the DMD dynamics matrix
X^+ = pseudoinverse of X
x = data vector
z = sinusoidal component of the data vector
λ = eigenvalue of the DMD dynamics matrix from the data with zero mean
μ = eigenvalue of the proxy matrix

I. Introduction

The technique of Pressure-Sensitive Paint (PSP) is commonly used in the aerospace industry to measure surface pressures on the model of launch vehicles and airplanes in the wind tunnel test (Refs. [1, 2]). Recent research has demonstrated that Unsteady Pressure-Sensitive Paint (uPSP) can be an essential tool for the assessment of the unsteady, aerodynamic phenomena (Refs. [3, 4, 5]). NASA is developing a new state-of-the-art uPSP capability in production wind tunnels (Refs. [6-16]). The work described in this paper is a part of the campaign.

This paper discusses the Dynamic Mode Decomposition (DMD) of the uPSP measurements, which were collected with four Phantom high-speed cameras at a constant sample frequency in the Ascent Transient Aerodynamics Test (ATAT) of the Space Launch System (SLS) Block 1 cargo vehicle with the Unitary Plan Wind Tunnel (UPWT) 11-by-11-foot Transonic Wind Tunnel in September 2019 at NASA Ames Research Center. Fig. 1 shows the scale model with uPSP in the SLS ATAT.

The conventional DMD algorithm is based on the Singular Value Decomposition (SVD). For the data with zero mean, the DMD is equivalent to the Discrete Fourier Transform (DFT). Since the uPSP is mainly used to determine the unsteady property of the aerodynamic flow, the DMD of the uPSP measurements is implemented in two steps: (1) subtract the mean value from the uPSP measurement; (2) apply the Fast Fourier Transform (FFT) on the resulting data with zero mean. The DMD outputs in this paper were generated with the execution in parallel of a code in C, with libraries of FFTW for FFT and MPI/OpenMP for parallel processing, on the NASA Pleiades supercomputer.

This paper is organized as follows. The DMD model and algorithm are described in Section 3. The equivalence of the DMD and the DFT for the data with zero mean is discussed in Section 3. In Section 4, the equivalence of the DMD and the DFT for the data with zero mean is verified with a sample uPSP data set, and the algorithm to implement the DMD to the uPSP measurements is discussed. In Section 5, the results of the DMD of the uPSP measurements in the tests of Mach sweep runs of the SLS ATAT are shown, and the effectiveness of the DMD of the uPSP measurements in the diagnosis of the unsteady, aerodynamic phenomena is demonstrated. Finally, the conclusions are presented in Section 6.

II. DMD Model and Algorithm

The DMD is based on the eigendecomposition of a best-fit linear operator that approximates the dynamics present in the data. Given the time series of data, DMD computes a set of modes, each of which is associated with a fixed oscillation frequency and growth/decay rate. The description of the DMD model and algorithm in this section is based on the papers by Schmidt (Ref. [17]) and Taira *et al*. (Ref. [18]).

Consider N data vectors collected at time t_k, k = 0, 1, …, N-1. Each of the data vectors has the dimension of M. For simplicity, it is assumed that the dimension of the vectors is larger than the number of vectors, i.e., $M > N$. As shown later in this paper, this assumption is true for the uPSP measurements collected in the SLS ATAT.

Let the data vectors be denoted as $\{x_k,\ \ k = 0, 1, \ldots, N-1\}$. The combined N data vectors form an $M \times N$ data matrix

$$D = [x_0 \quad x_1 \quad x_2 \quad \ldots\ldots \quad x_{N-2} \quad x_{N-1}] \tag{1}$$

In DMD, it is assumed the data vectors are separated by a constant interval of time, and the relationship between the consecutive vectors is given by the following equation

$$x_{k+1} = A\, x_k \qquad\qquad k = 0, 1, \ldots N\text{-}2. \tag{2}$$

where the linear operator, in the form of an $M \times M$ constant matrix A, approximates the dynamics of the system. In this paper, the matrix A is referred as the DMD dynamics matrix.

Equation (2) can be rewritten in the matrix form below

$$X^{\#} = AX \tag{3}$$

where X and $X^{\#}$ are $M \times (N-1)$ matrices defined as following

$$X = [x_0 \quad x_1 \quad x_2 \quad \ldots \quad \ldots \quad x_{N-2}] \tag{4}$$

$$X^{\#} = [x_1 \quad x_2 \quad x_3 \quad \ldots \quad \ldots \quad x_{N-1}] \tag{5}$$

The DMD dynamics matrix A can be determined as

$$A = X^{\#}X^{+} \tag{6}$$

where X^{+} denotes the pseudoinverse of X. Consider the dimension of the data vectors, M, is usually a large number, instead of determining the $M \times M$ matrix A, the DMD algorithm computes the eigenvalues and eigenvectors of the matrix A.

The conventional DMD algorithm, which is based on the SVD, includes the following steps:

First, perform the reduced SVD of X as following

$$X = U_r \Sigma_r V_r^T \tag{7}$$

where U_r and V_r are $M \times r$ and $N \times r$ matrices respectively. Σ_r is a $r \times r$ diagonal matrix, whose diagonal elements are non-zero singular values of the matrix X.

Then define a $r \times r$ proxy matrix $\tilde{A}$ as following

$$\tilde{A} = U_r^T A U_r = U_r^T X^{\#} V_r \Sigma_r^{-1} \tag{8}$$

and find the eigenvalues μ_j and eigenvectors $\tilde{v}_j$, j = 1, 2, …, r, of the proxy matrix $\tilde{A}$, with

$$\tilde{A}\tilde{v}_j = \mu_j \tilde{v}_j \tag{9}$$

Every non-zero eigenvalues μ_j is an eigenvalue of the DMD dynamics matrix A. The corresponding eigenvector of A, denoted as v_j, is determined as

$$v_j = \mu_j^{-1} X^{\#} V_r \Sigma_r^{-1} \tilde{v}_j \tag{10}$$

Each of the eigenvalues of the DMD dynamics matrix A defines the oscillation frequency and growth/decay rate of a DMD mode in time, and the corresponding eigenvector defines the shape of the DMD mode in space.

III. Equivalence of DMD and DFT for the Data with Zero Mean

It is proved that for the data with zero mean, the DMD is equivalent to the DFT. The discussion in this section is based on the papers by Rowley *et al* (Ref. [19]) and Chen *et al* (Ref. [20]).

For the data with zero mean, the sum of the elements of the data matrix D, given in Eq. (1), is zero for each row. Therefore, the following equation can be derived

$$x_0 + x_1 + x_2 + \cdots + x_{N-1} = 0 \tag{11}$$

From Eq. (2), the data vectors $\{x_k,\ \ k = 1, \ldots, N-1\}$ can be rewritten as

$$x_1 = Ax_0 \tag{12a}$$

$$x_2 = A^2 x_0 \tag{12b}$$

… …

$$x_{N-1} = A^{N-1} x_0 \tag{12c}$$

Combining equations (11) and (12) leads to

$$\begin{aligned} 0 &= x_0 + x_1 + x_2 + \cdots x_{N-1} \\ &= x_0 + Ax_0 + A^2 x_0 + \cdots + A^{N-1} x_0 \\ &= (I + A + A^2 + \cdots + A^{N-1}) x_0 \end{aligned} \tag{13}$$

Since x_0 is arbitrary, it is derived

$$I + A + A^2 + \cdots + A^{N-1} = 0 \tag{14}$$

Let λ denote an eigenvalue of the DMD dynamics matrix A, then λ satisfies the following equation

$$1 + \lambda + \lambda^2 + \cdots + \lambda^{N-1} = (1 - \lambda^N)/(1 - \lambda) = 0 \tag{15}$$

Therefore

$$\lambda_j = e^{i\frac{2\pi j}{N}} \qquad j = 1, 2, \ldots N\text{-}1 \tag{16}$$

where i is the imaginary unit.

It is shown for the data with zero mean, the eigenvalues of the DMD dynamics matrix are N-th roots of 1 (excluding 1 itself), which are uniformly located on the unit circle in the complex plane. The eigenvalue λ_j corresponds to a sinusoidal oscillation at the frequency

$$f_j = j \cdot f_s/N \qquad j = 1, 2, \ldots N\text{-}1 \tag{17}$$

where f_s is the sample frequency of the data.

IV. DMD of the uPSP Measurements

In this section, we discuss the implementation of DMD to the uPSP measurements of the SLS ATAT.

The uPSP measurements were collected with four Phantom high-speed cameras at a constant sample frequency in the SLS ATAT and then processed with the uPSP data processing software (Ref. [10, 12, 15]). The output is an $M \times N$ matrix of the nondimensional delta pressure coefficients at the nodes of a grid on the surface of the scale model. The DC component is subtracted in the time series of the delta pressure coefficient for each of the grid nodes. The number of rows, M, corresponds to the number of nodes in the grid, and the number of columns, N, corresponds to the number of camera output frames used in the DMD.

As a comparison to the SVD-based DMD algorithm, the DFT was also applied to the rows of the $M \times N$ matrix of the uPSP detla pressure coefficients, implemented with the FFT algorithm. Let W_j denote the M dimensional vector of the DFT coefficients corresponding to the eigenvalue $\{\lambda_j,\ j = 1, 2, \ldots, N-1\}$ given in Eq. (16), then the data vectors $\{x_k,\ k = 0, 1, \ldots, N-1\}$, i.e., the columns of the $M \times N$ matrix above, can be expressed with the eigenvectors W_j and eigenvalues λ_j as following

$$x_k = \sum_{j=1}^{N-1} z_{j,k} \tag{18}$$

where

$$z_{j,k} = W_j \lambda_j^k = W_j e^{i\frac{2\pi jk}{N}} \tag{19}$$

The vectors $\{z_{j,k},\ k = 0, 1, \ldots, N-1\}$ are the sinusoidal components of the data vectors $\{x_k,\ k = 0, 1, \ldots, N-1\}$ corresponding to the frequency $\{f_j,\ j = 1, \ldots, N-1\}$ given in Eq. (17).

Note that the elements of the vectors of the DFT coefficients, $\{W_j,\ j = 1, 2, \ldots, N-1\}$, are generally complex numbers. The conjugate complex vectors W_j and W_{N-j} (j = 1, 2, …, $\frac{N}{2} - 1$) define two sinusoidal oscillation modes, corresponding to the same frequency, which can be determined as $2Re(W_j)$ and $2Im(W_j)$, where $Re(W_j)$ and $Im(W_j)$ are real and imaginary parts of the vector W_j.

All the modes determined from the uPSP measurements are listed below

$$\left\{2Re(W_1), 2Im(W_1), 2Re(W_2), 2Im(W_2), \ldots\ldots, 2Re(W_{\frac{N}{2}-1}),\ 2Im\left(W_{\frac{N}{2}-1}\right), W_{\frac{N}{2}}\right\} \tag{20}$$

which correspond to the sinusoidal oscillations at the frequencies

$$f_j = j \cdot f_s/N \qquad j = 1, 2, \ldots, \frac{N}{2}. \tag{21}$$

Note that the vector $W_{\frac{N}{2}}$ is real, which corresponds to the Nyquist frequency

$$f_{Nyquist} = N/2 \cdot f_s/N = f_s/2 \tag{22}$$

A uPSP data set, with 128 frames of uPSP measurements of delta pressure coefficients on 341 grid nodes, is selected. The SVD-based DMD algorithm, as described in Eqs. (7)-(10), was applied to the uPSP data set before and after the mean is removed for each of the grid nodes. The DMD outputs are shown below, and the comparison between the outputs of the DMD and the DFT is provided as well.

Figs. 2(a) and 2(b) show the time series of the uPSP measurement of delta pressure coefficient on a sample grid node, before and after the mean is removed, respectively. In Fig. 2(a), the mean (0.00146) of the time series is an order of magnitude smaller than the standard deviation (0.011). Therefore, the time series of the delta pressure coefficient look almost the same before and after the mean is removed for a grid node. However, as shown below, the DMD outputs have different characteristics before and after the means are removed for all the grid nodes.

Figs. 3(a) and 3(b) show the 127 eigenvalues of the DMD dynamics matrix (denoted as blue crosses) in the complex plane, determined from the uPSP data set before and after the means are removed, respectively. The red circles show the 128th roots of 1 (excluding 1 itself), given in Eq. (16). For the uPSP data set before the means are removed, most of the eigenvalues of the DMD dynamics matrix are located close to the unit circle, indicating sinusoidal oscillations in the data; however, no obvious features are observed in the distribution of the eigenvalues. For the uPSP data set after the means are removed, the eigenvalues are equal to the 128th roots of 1 (excluding 1 itself), which are uniformly distributed in the unit circle in the complex plane.

Two sets of vectors of dimension 341 are computed for the uPSP data set, before and after the means are removed, respectively. The first set includes 127 eigenvectors of the DMD dynamics matrix determined with Eq. (10), and the second set includes 127 vectors of the DFT coefficients, determined from the FFT, of the uPSP data for each of the grid nodes. Both sets of 127 vectors are sorted in the ascending order of the phase of the corresponding eigenvalues, and the ratios of all elements of the corresponding vectors are computed. Note that the ratios are complex numbers since the elements of the vectors in both sets are complex. Figs. 4(a) and 4(b) show the real and imaginary parts of the ratios determined from the uPSP data set, before and after the means are removed, respectively. For the uPSP data set before the means are removed, no obvious features are observed in the ratios. However, when the means are removed, the ratios are constant complex numbers for all elements regarding each pair of the corresponding vectors in the two sets. In fact, the vectors of the DFT coefficients are also eigenvectors of the DMD dynamics matrix, which define the shape of DMD modes.

Figs. 3 and 4 verify the equivalence of the DMD and the DFT for the data with zero mean. Considering the uPSP measurements are mainly used to determine the unsteady property of the aerodynamic flow, the DMD of the uPSP measurements can be implemented in two steps:

(1) subtract the mean value from the uPSP measurement on each of the grid nodes;

(2) apply the FFT on the resulting zero-mean time series.

The DMD of the uPSP measurements with FFT has two advantages:

(1) The FFT algorithm is well known for its computational efficiency. For the time series of length N, the computational complexity of FFT is O(N*log$N$). Therefore, compared to the SVD-based DMD algorithm, the DMD with FFT reduces the computation time.

(2) Since the data size is big, it is advantageous to process the uPSP data in parallel. Compared to the SVD-based DMD algorithm, the DMD with FFT can be easily implemented in parallel processing.

V. Results of the SLS ATAT

The code to implement the DMD of the uPSP measurements was written in C, with libraries of FFTW for FFT and MPI/OpenMP for parallel processing. The DMD outputs were generated with the execution of the compiled C code in parallel on the NASA Pleiades supercomputer. In this section, the results of DMD of the uPSP measurements of the SLS ATAT are presented.

The data shown in this section are from two Mach sweep runs of the SLS ATAT. The first Mach sweep run was taken on the second day of the ATAT, and Mach number went from 0.70 to 1.00. The second Mach sweep run was taken on the third day of the ATAT, and Mach number went from 0.98 to 1.40. The attitude angles of the model were set to zeros in both Mach sweep runs.

In order to reduce the effect of the shot noise, a moving box filter with 5-by5-pixels was applied to each frame of the videos generated by four Phantom high-speed cameras. The uPSP measurements were then projected to a grid of 233,651 nodes on the surface of the scale model, and the first 1,024 frames were processed and the DMD outputs were generated.

The DMD of the uPSP measurements is effective in the diagnosis of the unsteady, aerodynamic phenomena in the SLS AUAT data. As examples, Figs. 5, 6 and 7 show the DMD modes of the vortex shedding at Mach numbers 0.80, 1.00 and 1.40, respectively. The vortex shedding was generated when the flow passed the connections between the core and the Solid Rocket Boosters (SRBs) of the SLS. In the plots (a) and (b) of each figure, the DMD modes corresponding to the real and imaginary parts of the vector of DFT coefficients were visualized on the surface of the model in 3D respectively. In the plot (c), the phase between the two corresponding DMD modes was shown in a plane of x coordinate and azimuth angle. The changes in the shape of the DMD modes can be observed when the test configuration went through the subsonic, transonic and supersonic regimes.

VI. Conclusions

This paper discusses the DMD of the uPSP measurements in the SLS ATAT with the UPWT 11-by-11-foot Transonic Wind Tunnel in September 2019 at NASA Ames Research Center. Since the uPSP is mainly used to determine the unsteady property of the aerodynamic flow, the DMD of the uPSP measurements is implemented with FFT, which has two advantages: (1) the FFT algorithm is well known for its computational efficiency, therefore, compared to the SVD-based DMD algorithm, the DMD with FFT reduces the computation time; (2) the DMD with FFT can be easily implemented in parallel processing. The DMD outputs were generated with the execution in parallel of a code in C, with libraries of FFTW for FFT and MPI/OpenMP for parallel processing, on the NASA Pleiades supercomputer. In this paper, the results of DMD of the uPSP measurements in the tests of Mach sweep runs of the SLS ATAT are presented, and the effectiveness of the DMD of the uPSP measurements in the diagnosis of the unsteady, aerodynamic phenomena is demonstrated.

Acknowledgement

Funding for this research was provided by the NASA Aeroscience Evaluation and Test Capabilities Project. The authors would like to thank James Bell, Paul Bremner, Nicholas Califano, Bob Ciotti, Ross Flach, Patrick Heaney, Kenji Kato, Bruce Laverde, Kenneth Lyons, Blair Mclachlan, Jack Ortega, Jayanta Panda, David Piatak, Victoria Pollard, James Ramey, Martin Sekula, Francesco Soranna, Thomas Steva, and Thomas Volden for their expertise and advices for the research work of this paper.

References

[1] Bell, J. H., Schairer, E. T., Hand, L. A., and Mehta, R.D., "Surface Pressure Measurements Using Luminescent Coatings", *Annual Review of Fluid Mechanics*, Vol. 33, No. 1, 2001, pp. 155-206.

[2] Liu, T. and Sullivan, J. P., *Pressure and Temperature Sensitive Paints*, Springer-Verlag, 2005.

[3] Gregory, J. W., Asai, K., Kameda, M., Liu, T., and Sullivan, J. P., "A Review of Pressure-Sensitive Paint for High-Speed and Unsteady Aerodynamics", *Proceedings of the Institution of Mechanical Engineers, Part G, Journal of Aerospace Engineering*, Vol. 222, No. 2, 2008, pp. 249-290.

[4] Gregory, J. W., Sakaue, H., Liu, T., and Sullivan, J. P., "Fast Pressure-Sensitive Paint for Flow and Acoustic Diagnostics", *Annual Review of Fluid Mechanics*, Vol. 46, 2014, pp. 303–330.

[5] Sellers, M. E., Nelson, M. A., and Crafton, J.W., "Dynamic Pressure-Sensitive Paint Demonstration in the AEDC Propulsion Wind Tunnel 16T", AIAA Paper 2016-1146, 54th AIAA Aerospace Sciences Meeting, San Diego, CA, January 2016.

[6] Schuster, D. M., Panda, J., Ross, J. C., Roozeboom, N. H., Burnside, N., Ngo, C. L., Kumagai, H., Sellers, M. E., Powell, J. M., Sekula, M. K., and Piatak, D. J., "Investigation of Unsteady Pressure-Sensitive Paint (uPSP) and a Dynamic Loads Balance to Predict Launch Vehicle Buffet Environments", NASA Engineering and Safety Center Report TI-14-00962, 2016.

[7] Roozeboom, N. H., Diosady, L. T., Murman, S. M., Burnside, N. J., Panda, J., and Ross, J. C., "Unsteady PSP Measurements on a Flat Plate Subject to Vortex Shedding from a Rectangular Prism", AIAA Paper 2016-2017, 54th AIAA Aerospace Sciences Meeting, San Diego, CA, January 2016.

[8] Panda, J., "Experimental Verification of Buffet Calculation Procedure Using Unsteady Pressure-Sensitive Paint", *Journal of Aircraft*, Vol.54, No. 5, 2017, pp. 1791-1801.

[9] Sellers, M. E., Nelson, M. A., Roozeboom, N. H., and Burnside, N. J., "Evaluation of Unsteady Pressure Sensitive Paint Measurement Technique for Space Launch Vehicle Buffet Determination", AIAA Paper 2017-1402, 55th AIAA Aerospace Sciences Meeting, Grapevine, TX, January 2017.

[10] Roozeboom, N. H., Ngo, C. L., Powell, J. M., Murakami, D. D., Ross, J. C., Murman, S. M., and Baerny, J. K., "Data Processing Methods for Unsteady Pressure-Sensitive Paint Application", AIAA 2018-1031, 56th AIAA Aerospace Sciences Meeting, Kissimmee, Florida, January 2018.

[11] Panda, J., Roozeboom, N.H., and Ross, J. C., "Wavenumber-Frequency Spectra on a Launch Vehicle Model Measured via Unsteady Pressure-Sensitive Paint", *AIAA Journal*, Vol. 57, No. 5, 2019, pp. 1801-1817.

[12] Roozeboom, N. H., Powell, J. M., Baerny, J. K., Murakami, D. D., Ngo, C. L., Garbeff, T. J., Ross, J. C., and Flach, R. L., "Development of Unsteady Pressure-Sensitive Paint Application on NASA Space Launch System", AIAA Paper 2019-3502, AIAA Aviation Forum, Dallas, TX, June 2019.

[13] Sekula, M. K., Piatak, D. J., Rausch, R. D., Ross, J. C., and Sellers, M. E., "Assessment of Buffet Forcing Function Development Process Using Unsteady Pressure Sensitive Paint", AIAA Paper 2019-3503, AIAA Aviation Forum, Dallas, TX, June 2019.

[14] Steva T. B., Pollard, V. J., Herron, A. J., and Crosby, W. A., "Space Launch System Aeroacoustics Wind Tunnel Test Results", AIAA Paper 2019-2202, AIAA Aviation Forum, Dallas, Texas, June 2019.

[15] Powell, J. M., Murman, S. M., Ngo, C. L., Roozeboom, N. H., Murakami, D. D., Baerny, J. K., and Li, J., "Development of Unsteady-PSP Data Processing and Analysis Tools for the NASA Ames Unitary 11ft Wind Tunnel", AIAA Paper 2020-0292, AIAA SciTech Forum, Orlando, FL, January 2020.

[16] Roozeboom, N. H., Murakami, D. D., Li, J., Powell, J. M., Baerny, J. K., Stremel, P. M., Volden, T. R., Flach, R. L., Douthitt, A. N., Steva, T. B., Ross, J. C., and Bell, J. H., "Recent Developments in NASA's Unsteady Pressure-Sensitive Paint Capability", AIAA Paper 2020-0516, AIAA SciTech Forum, Orlando, FL, January 2020.

[17] Schmidt, P.J., "Dynamic Mode Decomposition of Numerical and Experimental Data", *Journal of Fluid Mechanics*, Vol.656, Aug. 2010, pp.5-28.

[18] Taira, K., Brunton, S.L., Dawson, S. T. M., Rowley, C.W., Colonius, T., McKeon, B.J., Schmidt, O.T., Gordeyev, S., Theofilis, V., and Ukeiley, L.S., "Modela Analysis of Fluid Flows: An Overview", *AIAA Journal*, Vol.55, No.12, 2017, pp.4013-4041.

[19] Rowley, C.W., Mezić, I., Bagheri, S., Schlatter, P., and Henningson, D. S., "Spectral Analysis of Nonlinear Flows", *Journal of Fluid Mechanics*, Vol. 641, No. 1, 2009, pp. 115–127.

[20] Chen, K. K., Tu, J. H., and Rowley, C.W., "Variants of Dynamic Mode Decomposition: Boundary Condition, Koopman, and Fourier Analyses," *Journal of Nonlinear Science*, Vol. 22, No. 6, 2012, pp. 887–915.

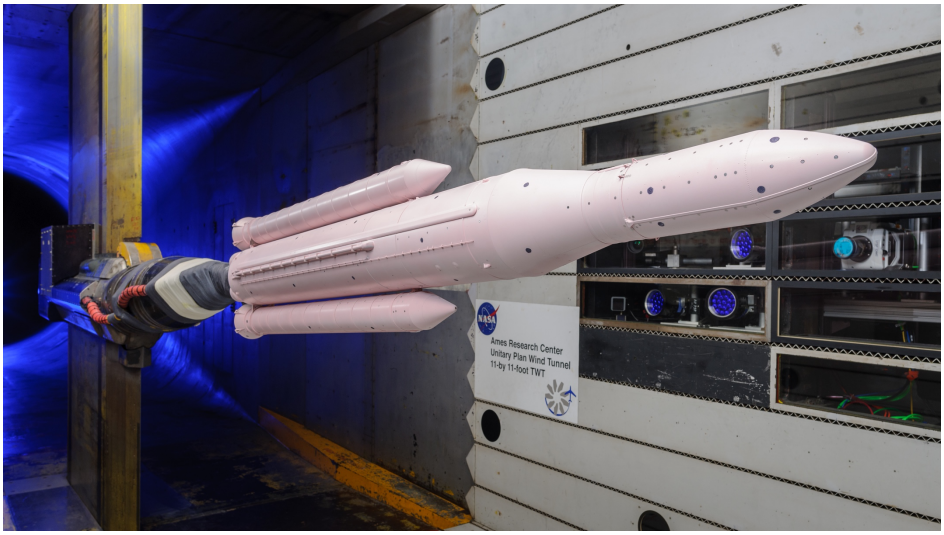

Fig. 1 Scale model of the SLS Block 1 cargo vehicle with uPSP in ATAT

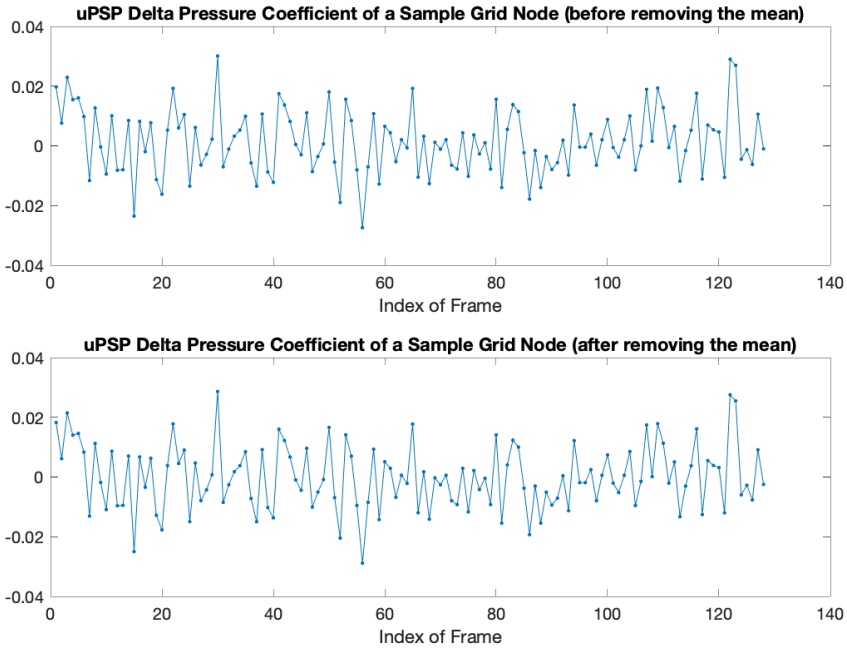

Fig. 2 Delta pressure coefficients of a sample grid node determined from the uPSP measurement: (a) before the mean is removed; (b) after the mean is removed.

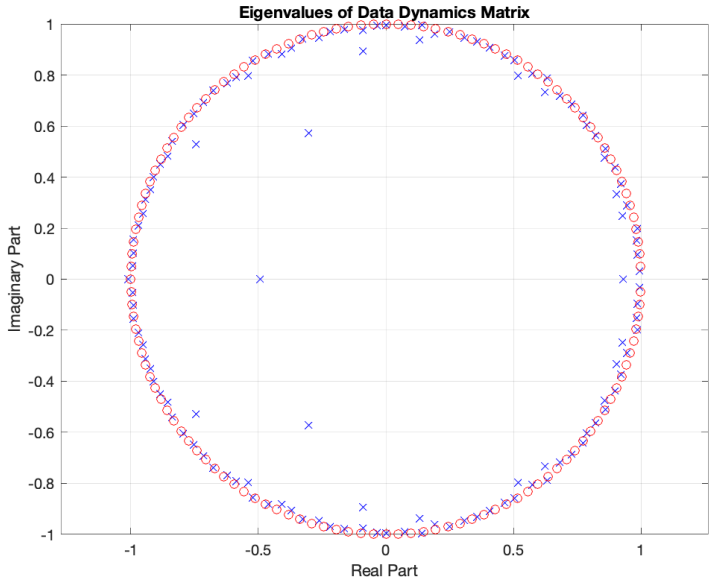

(a)

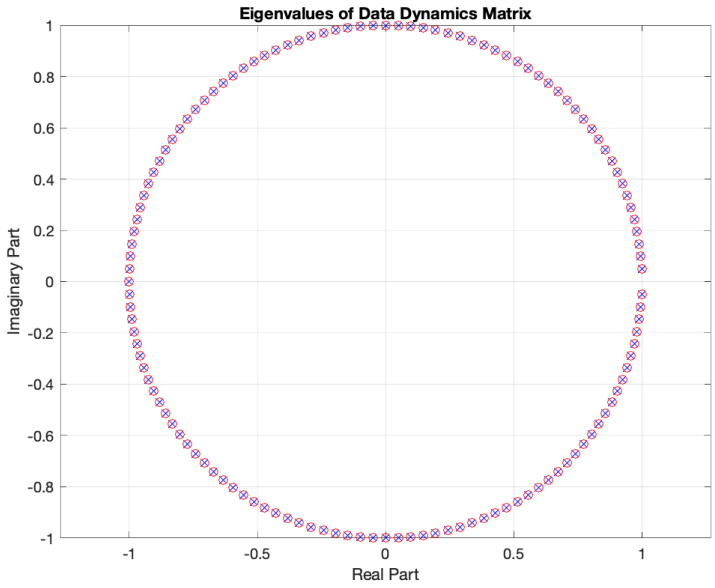

(b)

Fig. 3 Eigenvalues of the DMD dynamics matrix (denoted as blue crosses) from the sample data set of 128 frames of uPSP measurements on 341 grid nodes: (a) before the means are removed; (b) after the means are removed. The 128th roots of 1 (excluding 1 itself) are denoted as red circles.

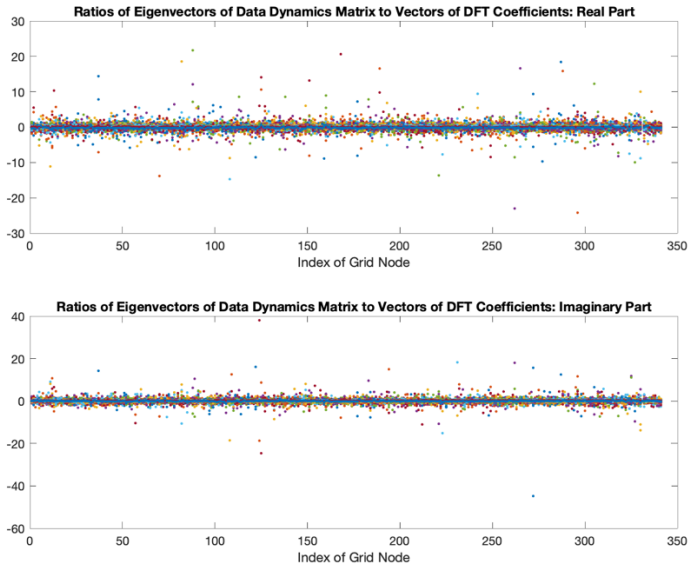

(a)

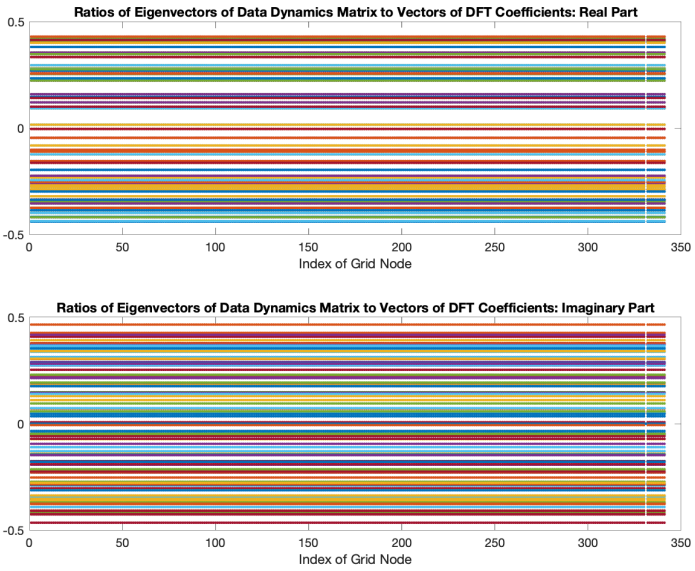

(b)

Fig. 4 Ratios of Eigenvectors of the DMD dynamic matrix to vectors of DFT coefficients from the sample data set of 128 frames of uPSP measurements on 341 grid nodes: (a) before the means are removed; (b) after the means are removed. In the plots of (a) and (b), the top and bottom subplots show the real and imaginary parts of the ratios respectively.

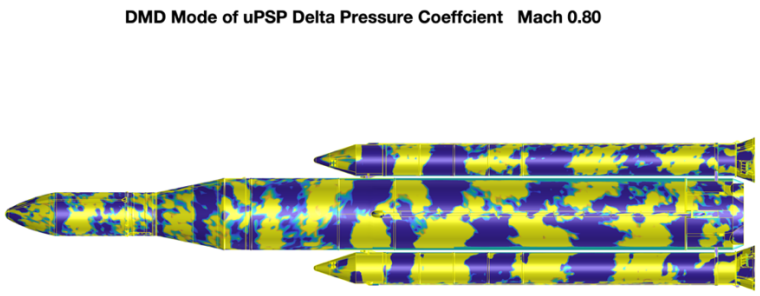

(a)

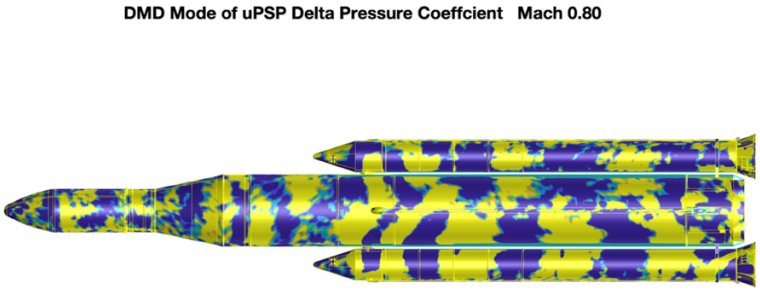

(b)

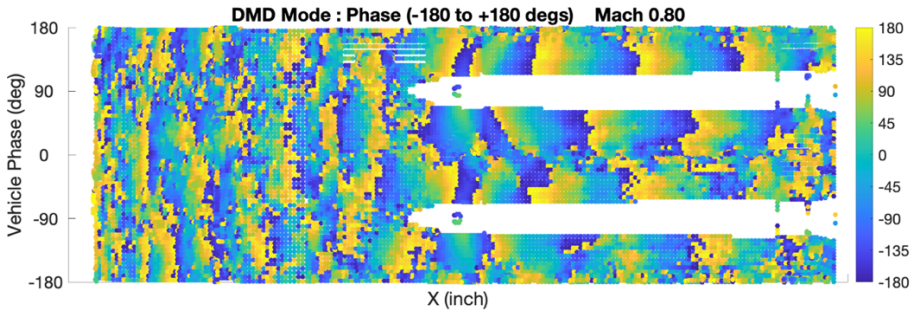

(c)

Fig. 5 DMD modes of vortex shedding in a test of Mach sweep runs of the SLS AUAT, where the Mach number was 0.80. The plots (a) and (b) show the DMD modes on the model, corresponding to the real and imaginary parts of the DFT coefficients respectively; the plot (c) shows the phase of the two DMD modes in the plane of x coordinate and azimuth angle.

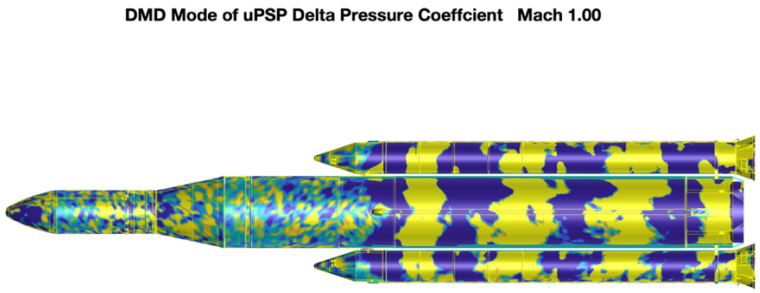

(a)

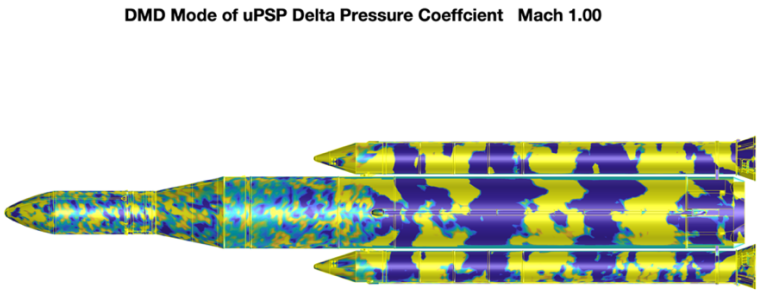

(b)

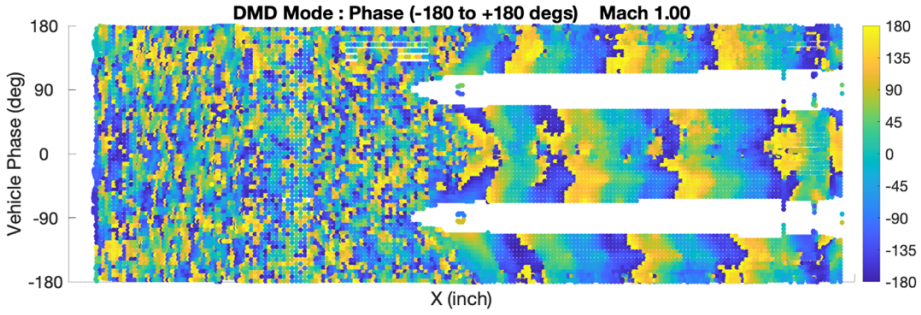

(c)

Fig. 6 DMD modes of vortex shedding in a test of Mach sweep runs of the SLS AUAT, where the Mach number was 1.00. The plots (a) and (b) show the DMD modes on the model, corresponding to the real and imaginary parts of the DFT coefficients respectively; the plot (c) shows the phase of the two DMD modes in the plane of x coordinate and azimuth angle.

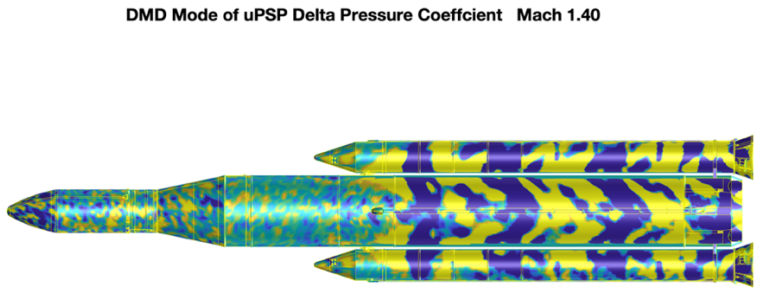

(a)

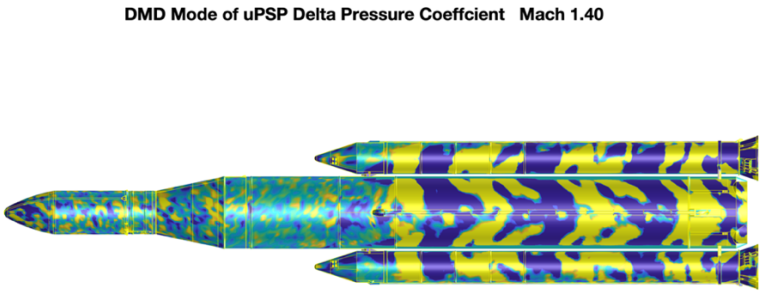

(b)

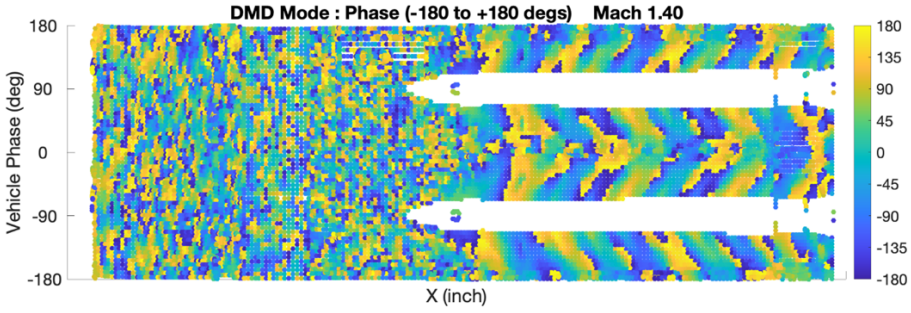

(c)

Fig. 7 DMD modes of vortex shedding in a test of Mach sweep runs of the SLS AUAT, where the Mach number was 1.40. The plots (a) and (b) show the DMD modes on the model, corresponding to the real and imaginary parts of the DFT coefficients respectively; the plot (c) shows the phase of the two DMD modes in the plane of x coordinate and azimuth angle.